# MULTI-LEVEL MEAN-SHIFT CLUSTERING FOR SINGLE-CHANNEL RADIO FREQUENCY SIGNAL SEPARATION

*Yi Zhou*[†]*, Yi Feng, Vahid Tarokh*

Department of ECE, Duke University
Teer Engineering Box Building
Durham, NC 27708, USA

*Vadas Gintautas*[*]*, Jessee McClelland, Denis Garagic*

BAE Systems FAST Labs
600 District Ave
Burlington, MA 01803, USA

## ABSTRACT

Emerging wireless communication applications have led to a crowded radio frequency (RF) spectrum. Therefore, it is desired to develop signal separation techniques that can extract different RF signals from their mixtures. Existing signal separation approaches typically require multiple observations of the signal mixtures and depend on statistical independence among the signals. In this paper, we consider separating multiple RF wireless signals from their single-channel superposition. These RF signals are transmitted in their corresponding high-frequency pass bands with diverse power spectrum densities, bandwidths, and time durations. We propose a signal separation approach that exploits the mean-shift clustering algorithm with multiple levels of cluster sizes to identify RF signals with different bandwidths in the spectrogram of the superposed signal. We demonstrate the effectiveness of our approach by separating RF signals using real datasets.

***Index Terms—*** Single-channel signal separation, radio frequency, mean-shift clustering

## 1. INTRODUCTION

Single-channel source separation techniques have been well developed for various signal processing applications, e.g., [1–5]. In these applications, the problem is to separate individual source signals from a single observation of their superposition, i.e.,

$$\boldsymbol{y} = \boldsymbol{s}_1 + \boldsymbol{s}_2 + \cdots + \boldsymbol{s}_k, \tag{1}$$

where $\{\boldsymbol{s}_i\}_{i=1}^k$ denote time series data that correspond to $k$ different source signals and $\boldsymbol{y}$ is the superposed signal. In this paper, we consider the scenario where each source signal $\boldsymbol{s}_i, i = 1, ..., k$ corresponds to a specific type of wireless radio frequency (RF) signal, such as WiMAX (Worldwide Interoperability for Microwave Access), Wi-Fi (wireless local area networking), DECT (Digital Enhanced Cordless Telecommunications), and various UAS (unmanned aicraft systems) radio protocols. Such a model simulates the wireless transmissions in the air where the RF signals are superposed with each other and we can only observe the superposed signal. As the RF spectrum is becoming crowded, it is desired to develop RF surveillance techniques that can monitor the channel activities and help to improve the efficiency of channel resource allocation. Therefore, the goal of this paper is to develop an algorithm that can infer the individual RF source signals from such a single-channel observation of the superposed signal.

It is natural to consider applying existing single-channel source separation techniques to extract the individual RF source signals from their mixture. However, these approaches depend on certain statistical structures of the underlying source signals that are not available for RF signals. Specifically, many works propose single-channel source separation methods based on independent component analysis (ICA)-related techniques [3–10], which exploit the statistical independence among the source signals. However, some RF signals occupy a wide frequency band that contains multiple independent subcarriers, and we need to group these independent components (instead of separating them) as one source signal. Other works propose tensor factorization-based approaches for source separation [1, 2, 9, 11–14]. These approaches require transforming the single-channel observation into multiple channels, and the separation performance is sensitive to the transformation parameters. Also, tensor factorization requires to solve a highly nonconvex optimization problem, which in general has many local minima and saddle points [15]. Other single-channel source separation approaches are based on statistical structures such as sparsity and low-rankness [16–22], which is not a prominent feature of RF signals. The challenges for RF signal separation can be summarized as follows.

- **Diverse signal bandwidth:** RF signals occupy very different signal bandwidths that vary from 1 Mhz to 20 Mhz and beyond.
- **Diverse signal duration:** RF signals have very different

† Corresponding author. Email: yi.zhou610@duke.edu

*Approved for public release; unlimited distribution. Not export controlled per ES-FL-060519-0124.

signal duration time. For example, the UAS signal lasts for milliseconds while the WiMAX signal can last for seconds. Therefore, the separation approach should be able to identify these signals at very different time scales.

- **Diverse power spectral density:** RF signals are transmitted by various devices located in different places. The received signal power spectral densities are greatly affected by the distances between the transmitters and the receiver. Therefore, the separation approach should be able to identify the signals at different scales of power spectral density.

Figure 1 shows the spectrogram of a superposed signal that consists of three types of RF signals (i.e., DECT, WiMAX and UAS) obtained by short time Fourier transform (STFT). Note that to simulate the crowed RF channel, we have generated multiple copies of each source signal and assigned them with random center frequencies as well as random start time. The goal is to identify the frequency band and the start/end time of each RF signal, in order to separate each signal from the complex RF spectrum background.

In this paper, we propose a source separation method for extracting RF signals from their single-channel superposition. Our approach can identify the individual RF signals in the complex wireless environment that is described above. In particular, unlike most traditional single-channel source separation approaches that exploit the signal statistics only in the time domain, our approach exploits the cluster structure of power spectral density of the RF signals in the time-frequency domain and leverages the mean-shift clustering algorithm to identify the frequency bands as well as time intervals of different RF signals.

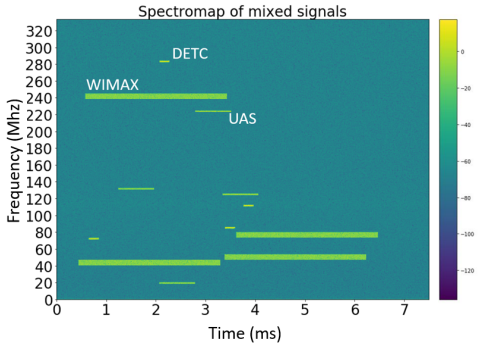


**Fig. 1**. Spectrogram of a superposition of three types of RF signals: WiMAX, DECT and UAS.

## 2. MEAN-SHIFT CLUSTERING FOR SINGLE TYPE OF RF SIGNAL SEPARATION

In this section, we first introduce the basic mean-shift clustering algorithm, based on which we further propose an approach to separate a single type of RF signal from the background spectrum.

### 2.1. Mean-shift Clustering Algorithm

Mean-shift clustering is a non-parametric machine learning algorithm for identifying clusters of points in the high-dimensional space [23]. To elaborate on a basic version of mean-shift clustering algorithm, consider the task of clustering a set of points $\{x_1, x_2, ..., x_n\}$ in $\mathbb{R}^d$, where each point $x_i$ is associated with a nonnegative weight $w_i \in \mathbb{R}_+$. The mean-shift clustering algorithm initializes a cluster ball $\mathcal{B}_r(O)$ centered at an initialization point $O \in \mathbb{R}^d$ with a pre-specified radius $r > 0$. Then, in each update step, the algorithm moves the center $O$ of the cluster ball to the gravity center of the points that are included within the ball at the current step. The update rule for mean-shift clustering algorithm can be formally written as:

$$O \leftarrow \frac{\sum_{x_i \in \mathcal{B}_r(O)} w_i \|x_i - O\|^2}{\sum_{x_i \in \mathcal{B}_r(O)} \|x_i - O\|^2}. \quad (2)$$

Intuitively, the algorithm follows the gradient of the weighted density of the data points and moves the cluster ball to achieve a local maximum of the total weights of the included points. Figure 2 provides an illustration of the application of mean-shift clustering to cluster a set of blue points in the 2-D plane. The cluster ball (i.e., red circle) is initialized at the boundary of the points with certain radius $r$, and the green curve denotes the path that the cluster center takes along the mean-shift updates.

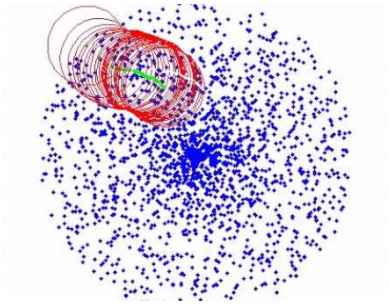

**Fig. 2**. Illustration of mean-shift clustering.

The mean-shift clustering algorithm does not need to specify the number of clusters. In practice, one can initialize a set of clustering balls centered at different locations to explore various local maxima of the weighted density in the entire space. The cluster radius $r$ of the cluster ball is a parameter of the algorithm that is tuned according to the dataset.

### 2.2. Separate RF Signal via Mean-shift Clustering

In this subsection, we propose a mean-shift clustering-based approach to separate a single type of RF signal from the background spectrum based on a single-channel observation. As an illustrative example, Figure 3 shows the short time Fourier transform (STFT) of a WiMAX signal with bandwidth approximately 7Mhz. The power spectral densities (PSD) of the

signal and the background spectrum are denoted by different colors according to the decibel values. The goal is to identify the frequency band and the start & end time of the RF signal, and our approach is based on applying the mean-shift clustering to the STFT matrix.

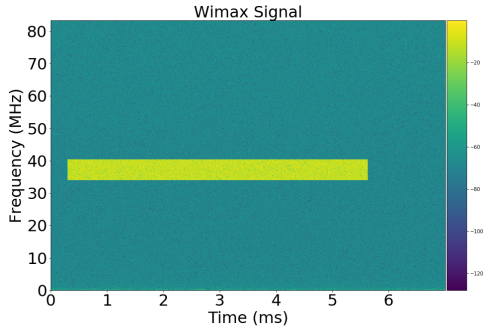


**Fig. 3**. Spectrogram of WiMAX signal.

Specifically, to separate the WiMAX spectrum from the background spectrum as shown in Figure 3, our approach consists of the following key steps.

**Step 1): Cluster spectrum for each time unit**

We first consider the entire spectrum at each time unit, i.e., every column of the STFT matrix as shown in Figure 3. Suppose each column $\boldsymbol{z}$ of the STFT matrix has $n$ coordinates $\boldsymbol{z} = [z_1, ..., z_n]$. The coordinate indices $1, ..., n$ denote the locations of the coordinates to be clustered, and their corresponding power spectral density values $z_1, ..., z_n$ denote the associated weights of these coordinates. Then, we apply the mean-shift clustering algorithm to cluster these $n$ coordinates based on their power spectral densities. Specifically, we initialize a set of non-overlapping cluster intervals that cover the entire spectrum $\boldsymbol{z}$ at each time unit, and the length of the intervals $r$ are set to be the bandwidth of WiMAX. Figure 4 (a) illustrates the initialization scheme for the mean shift clustering applied to one column of the STFT matrix. Note that the two red cluster intervals are initialized around the WiMAX frequency band.

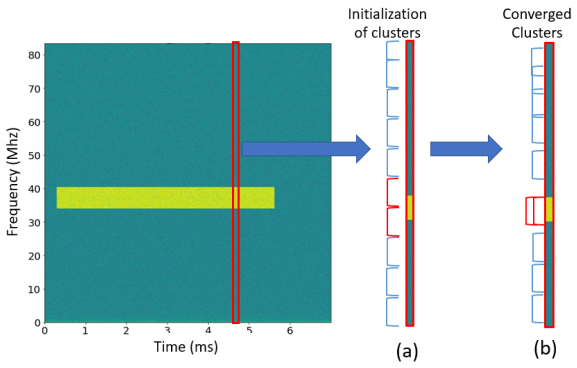


**Fig. 4**. Application of mean-shift clustering to RF spectrum at a given time. (a): initialization of the cluster intervals. (b): illustration of cluster intervals after convergence.

Next, we update the cluster center of each initialized cluster interval according to eq. (2) until convergence is achieved, which is illustrated in Figure 4 (b). Intuitively, the red cluster intervals that are initialized around the WiMAX frequency band converge to the frequency band of WiMAX, while other cluster intervals converge to some random locations of the background spectrum.

**Step 2): Identify signal pattern from the clustering result**

We apply the mean-shift clustering procedure described in step 1 to all the columns of the STFT matrix. Figure 5 shows the clustering result, which denotes a binary matrix with the 1s (i.e., black dots) correspond to the center of the cluster intervals after convergence of the algorithm.

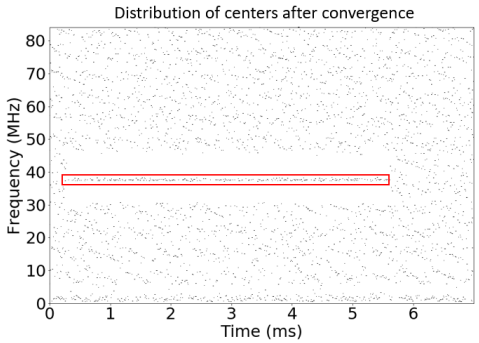


**Fig. 5**. Distribution of cluster center results of mean-shift clustering applied to a spectrogram. Black dots denote the centers of cluster intervals.

One can see from the clustering result in Figure 5 that the high power spectral density within the frequency band of the WiMAX signal attracts the centers of the surrounding cluster intervals to converge to the center frequency along the time axis (as shown within the rectangle in Figure 5). In comparison, the centers of the cluster intervals that are in the background spectrum take a random walk. Therefore, we can identify the signal frequency band by locating the centers of the cluster intervals that form a stable horizontal line pattern along the time axis. Specifically, we search for a horizontal line-like pattern in the binary matrix shown in Figure 5 that lasts for at least $t = 30$ time units along the time axis with fluctuations in the frequency axis less than $v = \frac{r}{5}$ (recall that $r$ denotes the cluster interval length). These parameter settings are empirically found to lead to a stable performance. In particular, such a search can be realized by applying a rectangular window with size $t \times v$ to scan over the binary matrix in Figure 5 and remove the cluster centers which lead to discontinuities of the pattern within the rectangular window. The parameters $t$ and $v$ determine the thresholds for identifying a signal pattern, and they are tuned according to the specific scenario. In our experiments, we found that choices of $t \in [20, 30]$ and $v \in [\frac{r}{5}, \frac{r}{3}]$ provide satisfactory results. After filtering out the centers that do not form a horizontal line-like pattern, we set the entries included within their corresponding

cluster intervals to be one. Such a binary separation matrix denotes the frequency band that each RF signal lies in along the signal duration time.

### 2.3. Experiments

We apply our proposed approach to separate a superposition of multiple copies of a single type of RF signal with random center frequencies, power spectral densities and start times. The first row of Figure 6 shows the spectrogram of such superposed DECT and UAS signals, respectively. The goal is to generate a binary separation matrix based on the spectrogram that indicates the locations of the RF signals in the frequency-time space. To evaluate the performance of our approach, we generate a ground truth binary matrix $M_{\text{true}}$ based on the spectrogram, in which the corresponding regions of the RF signals in the spectrogram are set to be 1. Then, we apply our approach to separate the superposed RF signals as shown in the first row of Figure 6. The cluster interval length is set to be the bandwidth of the corresponding type of RF signal. The second row shows the binary separation matrix $\overline{M}$ obtained by our approach. As shown in the figure, this approach successfully identifies all the RF signals components in different frequency bands and at different times. In particular, we compute the probability of detection (PD) and probability of false alarm (PF) by comparing the ground truth binary matrix and the binary separation matrix:

$$\text{PD} = \frac{\langle M_{\text{true}}, \overline{M} \rangle}{\texttt{nnz}(M_{\text{true}})}, \quad \text{PF} = 1 - \frac{\langle M_{\text{true}}, \overline{M} \rangle}{\texttt{nnz}(\overline{M})}, \qquad (3)$$

where $\texttt{nnz}(M)$ denotes the number of nonzero entries of a matrix $M$. In these two experiments, the PDs are above $97\%$ and the PFs are below $25\%$. This demonstrates the effectiveness of our approach in separating the RF signals from the background spectrum. It is possible to estimate other information such as center frequency, bandwidths and start/end times of the individual RF signals based on the horizontal and vertical coordinates of the binary separation matrix.

## 3. MULTI-LEVEL MEAN-SHIFT CLUSTERING FOR MULTIPLE TYPES OF RF SIGNAL SEPARATION

The previous section explains the application of mean-shift clustering to separate a single type of RF signal from its single-channel superposition. In practical scenarios, the superposed signal consists of multiple types of RF signals with diverse bandwidths. To handle complex scenarios such as this, we next generalize the previously proposed approach to adopt multiple levels of clustering intervals.

Specifically, we apply the mean-shift clustering-based approach multiple times with each time adopting a different cluster interval length to extract RF signals with a similar bandwidth. For example, suppose the superposed signal consists of three types of RF signals with bandwidths $r_1, r_2, r_3$, respectively. Then, we apply the mean-shift clustering-based approach introduced in Section 2 with cluster interval length

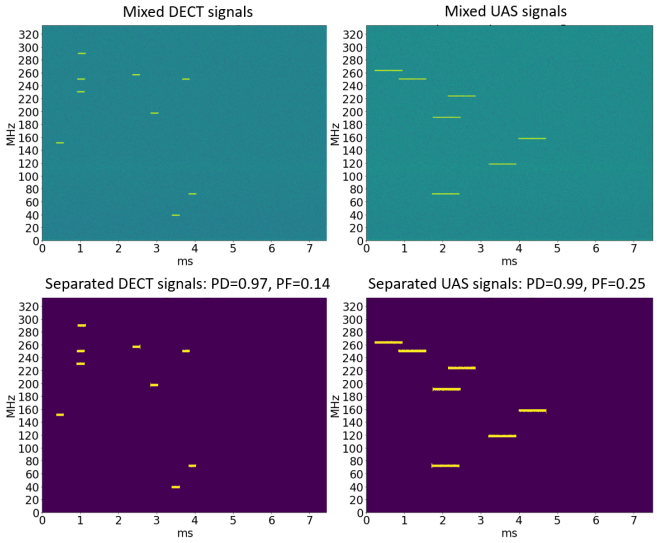


**Fig. 6**. Separation of superposed single type of RF signals.

set to be $r_1, r_2, r_3$, respectively, to identify the RF signals with the corresponding bandwidths. Ideally, we expect that the algorithm with different cluster interval lengths can extract the RF signals with the corresponding bandwidths. In particular, we need to pay further attention to the following issues.

- **Choosing proper cluster sizes:** In a practical wireless environment, the types of RF signals are typically unknown a priori and so are their bandwidths. Therefore, one cannot provide exact values for the cluster interval lengths used in our proposed multi-level mean-shift clustering algorithm. In practice, we can have a rough estimate of the maximum bandwidth $r_{\text{max}}$Mhz of the RF signals (e.g., 20 Mhz). Then, we choose the cluster interval lengths to span the parameter regime $(0, r_{\text{max}}]$ with a certain stepsize (e.g., 5 Mhz). Intuitively, more cluster levels can separate the RF signals at a finer granularity but introduce additional computation overhead.
- **Duplicate detections:** It is possible that a narrow band RF signal can be simultaneously identified by the mean-shift clustering-based approach with two different cluster sizes, e.g., a small cluster size and a large cluster size. This results in a confusion of whether the signal is of narrow band or wide band. In such a case, we always keep the separation result obtained by using the smallest cluster size and ignore results obtained by other larger cluster sizes.

### 3.1. Experiments

We generate synthetic datasets by superposing multiple RF signals with different bandwidths. To simulate a crowded channel, we assign random center frequencies and signal start times to different copies of these RF signals. The top row in Figure 7 shows the spectrogram of single-channel time series data that consists of three types of RF signals: WiMAX, DECT and UAS. These signals have diverse bandwidths and

signal duration times.

Since the maximum bandwidth of these signals is 7Mhz, we apply our multi-level mean-shift clustering approach with the cluster interval length set to be $2, 4, 7$ Mhz, respectively. The bottom row in Figure 7 presents the binary separation matrix obtained by our proposed multi-level mean-shift clustering approach. One can see from the result that our approach successfully identifies all individual RF signals in different frequency bands. In particular, our multi-level separation approach can separate RF signals with a cluster interval length similar to their bandwidths. This demonstrates that such a multi-level approach can separate RF signals at different scales of both frequency and time.

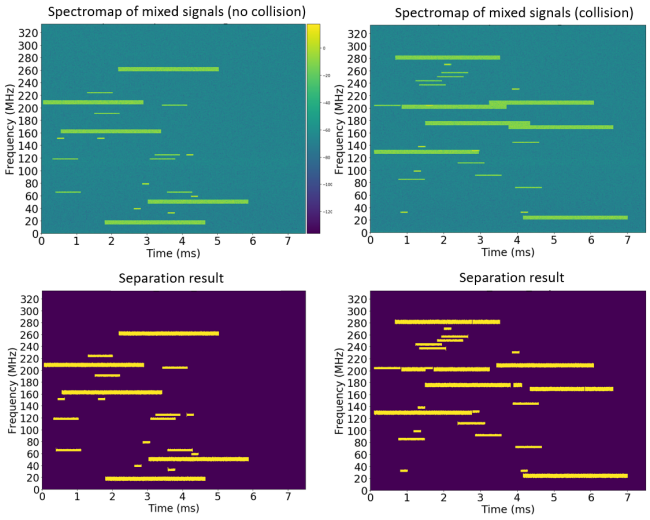


**Fig. 7**. Separation of superposed multiple types of RF signals.

We further generate 100 trials of this type of mixed spectrograms for the experiment. In the spectrogram of each trial, the numbers of WiMAX, DECT and UAS signals are drawn randomly up to 4,8 and 10, respectively. The starting times and center frequencies of these signals are also randomly generated to be within the range of the spectrogram. The cluster interval sizes of multi-level mean-shift clustering algorithm are set to be 2, 4 and 7 MHz. Figure 8 shows the scatter map of the PD and PF pairs of all the trials. In particular, the average detection rate is $95.3\%$, and more than $85\%$ of the trials achieve PD$>$0.9 and PF$<$0.3 (points within the rectangle). We also note that there are a few trials that have low detection rate and a relatively high false alarm. This is due to the interference/collision of signals in these randomly generated spectrograms. When signals interfere with each other in the spectrogram, mis-detections and false alarms occur and degrade the performance of the multi-level mean-shift clustering algorithm.

Lastly, we further test the sensitivity of the performance of multi-level mean-shift source separation algorithm with respect to the signal-to-noise ratio (SNR). To further illustrate

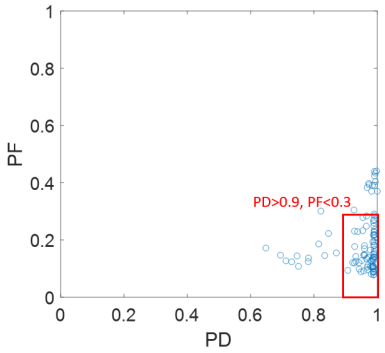


**Fig. 8**. Scatter map of (PD, PF) of 100 random experiments. The red rectangle collects the experiments (87 out of 100) that achieve a PD higher than $90\%$ and a PF lower than $30\%$.

the effectiveness of our algorithm, we compare the performance between our algorithm and a baseline approach that detects the binary separation matrix based on a pre-specified threshold. Specifically, we set the threshold for the baseline approach to be the average PSD of the entire mixed signal, i.e., the average value of the PSD spectrogram matrix. We think this is a reasonable setup as the average PSD of each individual RF signal is unknown a priori.

Then, for the comparison experiment, we fix a randomly generated spectrogram, and compute the SNR as the ratio between the average power spectral density of all signals and that of the background spectrum. We scale the background spectrum to have SNR ranging from 0 dB to 20 dB and test the performance of both our algorithm and the baseline approach. Figure 9 shows the result. One can see that our algorithm achieves a good performance (PD$>$0.90 & PF$<$0.12) when the signal power is 5 dB higher than the background spectrum. This demonstrates that our algorithm is robust to a reasonable amount of noise. On the other hand, one can see that the PD of the baseline approach outperforms ours in the low SNR regime (SNR$\leq$ 5dB), but its PF is much higher (more than $90\%$) than ours. This implies that the baseline approach simply claims most of the spectrogram as signals to achieve a high PD at the cost of sacrificing PF. In the high SNR regime, our algorithm achieves a higher PD than that of the baseline approach while suppressing the PF to be at a much lower level than that of the baseline approach.

## 4. CONCLUSION

In this paper, we propose a multi-level mean-shift clustering-based source separation algorithm to separate multiple RF signals from their single-channel superposition. These RF signals are transmitted in their corresponding high-frequency pass bands with diverse power spectrum densities, bandwidths, and time durations. We demonstrate that our algorithm can identify RF signals at different bandwidth scales as well as time scales. In future work, we plan to further facilitate the convergence of the algorithm by leveraging the

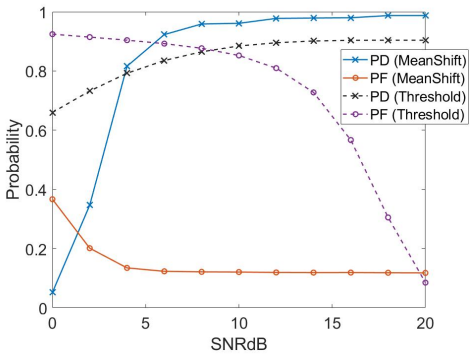


**Fig. 9**. Effect of SNR on PD & PF of our mean-shift based algorithm and a baseline threshold-based algorithm.

time-domain dependence and exploiting distributed implementation.

## Acknowledgments

Yi Feng's research is supported by the postdoctoral research fellowship from Fonds de recherche du Quebec - Nature et technologies.

### 5. REFERENCES

[1] B. Gao, *Single channel blind source separation*, Ph.D. thesis, Newcastle University, April 2011.

[2] E. S. Warner and I. K. Proudler, "Single-channel blind signal separation of filtered MPSK signals," *IEE Proceedings - Radar, Sonar and Navigation*, vol. 150, no. 6, pp. 396–402, Dec 2003.

[3] M. Davies and C. James, "Source separation using single channel ICA," *Signal Processing*, vol. 87, pp. 1819–1832, Aug 2007.

[4] B. Mijovic, M. De Vos, I. Gligorijevic, J. Taelman, and S. Van Huffel, "Source separation from single-channel recordings by combining empirical-mode decomposition and independent component analysis," *IEEE Transactions on Biomedical Engineering*, vol. 57, no. 9, pp. 2188–2196, Sep. 2010.

[5] G. Lu, M. Xiao, P. Wei, and J. Li, "Single channel blind separation of oversampling communication signals based on ICA," in *Proc. IEEE International Conference on Communiction Problem-solving*, Dec 2014, pp. 364–367.

[6] G. Jang, T. Lee, and Y. Oh, "Blind separation of single channel mixture using ICA basis functions," Jan 2002.

[7] G. Jang and T. Lee, "A maximum likelihood approach to single-channel source separation," *Journal of Machine Learning Research*, vol. 4, pp. 1365–1392, Dec. 2003.

[8] J. Heeris, *Single Channel Blind Source Separation Using Independent Subspace Analysis*, Ph.D. thesis, The University of Western Australia, Oct. 2007.

[9] E. M. Grais, M. Sen, and H. Erdogan, "Deep neural networks for single channel source separation," 2014, pp. 3734–3738.

[10] G. Lu, M. Xiao, P. Wei, and H. Zhang, "A new method of blind source separation using single-channel ICA based on higher-order statistics," *Mathematical Problems in Engineering*, vol. 2015, 2015.

[11] S. Kouchaki, S. Sanei, E. L. Arbon, and D. Dijk, "Tensor based singular spectrum analysis for automatic scoring of sleep EEG," *IEEE Transactions on Neural Systems and Rehabilitation Engineering*, vol. 23, no. 1, pp. 1–9, Jan 2015.

[12] D. Yang, C. Yi, Z. Xu, Y. Zhang, M. Ge, and C. Liu, "Improved tensor-based singular spectrum analysis based on single channel blind source separation algorithm and its application to fault diagnosis," *Applied Sciences*, vol. 7, no. 4, 2017.

[13] B. Wang and M. Plumbley, "Investigating single-channel audio source separation methods based on non-negative matrix factorization," in *Proc. ICA Research Network International Workshop*, Sep 2006, pp. 17–20.

[14] A. Phan, P. Tichavský, and A. Cichocki, "Blind source separation of single channel mixture using tensorization and tensor diagonalization," in *Proc. Latent Variable Analysis and Signal Separation*, 2017, pp. 36–46.

[15] Y. Zhou and Y. Liang, "Critical points of linear neural networks: Analytical forms and landscape properties," in *Proc. International Conference on Learning Representations (ICLR)*, 2018.

[16] E. J. Candès and J. Romberg, "Quantitative robust uncertainty principles and optimally sparse decompositions," *Foundations of Computational Mathematics*, vol. 6, no. 2, pp. 227–254, 2006.

[17] H. Zhang, Y. Zhou, and Y. Liang, "Analysis of robust pca via local incoherence," in *Advances in Neural Information Processing Systems*, pp. 1810–1818. 2015.

[18] E. J. Candès., X. Li, Y. Ma, and J. Wright, "Robust principal component analysis?," *Journal of the ACM*, vol. 58, no. 3, pp. 11:1–11:37, 2011.

[19] J. Wright, A. Ganesh, K. Min, and Y. Ma, "Compressive principal component pursuit," in *IEEE International Symposium on Information Theory*, July 2012, pp. 1276–1280.

[20] D. L. Donoho and G. Kutyniok, "Microlocal analysis of the geometric separation problem," *Communications on Pure and Applied Mathematics*, vol. 66, no. 1, pp. 1–47, 2013.

[21] M. McCoy, *A geometric analysis of convex demixing*, Ph.D. thesis, California Institute of Technology, 2013.

[22] Y. Zhou and Y. Liang, "Demixing sparse signals via convex optimization," in *Proc. IEEE International Conference on Acoustics, Speech and Signal Processing (ICASSP)*, March 2017, pp. 4202–4206.

[23] Y. Cheng, "Mean shift, mode seeking, and clustering," *IEEE Transactions on Pattern Analysis and Machine Intelligence*, vol. 17, no. 8, pp. 790–799, August 1995.